Polymer 51 (2010) 1494–1500

Contents lists available at ScienceDirect

Polymer

journal homepage: www.elsevier.com/locate/polymer

Morphology development and exclusion of noncrystalline polymer during crystallization in PVDF/PMMA blends

Yoshifumi Okabe [a], Hideki Murakami [b], Noboru Osaka [a], Hiromu Saito [a,*], Takashi Inoue [c]

[a] Department of Organic and Polymer Materials Chemistry, Tokyo University of Agriculture and Technology, Koganei-shi, Tokyo 184-8588, Japan
[b] Department of Organic and Polymeric Materials, Tokyo Institute of Technology, 2-12-1 Ookayama, Meguro-ku, Tokyo 152-8552, Japan
[c] Department of Polymer Science and Technology, Yamagata University, Jonan, Yonezawa-shi, Yamagata 992-8510, Japan

ARTICLE INFO

Article history:
Received 6 October 2009
Received in revised form
6 January 2010
Accepted 25 January 2010
Available online 2 February 2010

Keywords:
Light scattering
Atomic force microscopy
Crystallization

ABSTRACT

Morphology development during the crystallization of poly(vinylidene fluoride) (PVDF)/poly(methyl methacrylate) (PMMA) blends was investigated at various crystallization temperatures (T_C) by means of time-resolved light scattering measurements and atomic force microscopy (AFM). A coarse spherulite obtained at a high T_C of 162 °C was found to be developed with a two-step crystallization process. The ordering in the spherulites (*Pr*) increased with time at the early stages and then decreased at the later stages. The rate of spherulite growth started to decrease when *Pr* started to decrease. In contrast, in the compact spherulite obtained at a low T_C of 148 °C, *Pr* decreased monotonously with time while the growth rate was constant. AFM observation revealed that such characteristic crystallization behavior is attributed to the exclusion of PMMA from the crystal growth during the crystallization; i.e., the amount of excluded PMMA becomes larger as the distance from the spherulite center increases and the crystallization temperature rises.

1. Introduction

In mixtures of crystalline and noncrystalline components, the noncrystalline component can diffuse away from a crystal growth front; i.e., exclusion takes place. The exclusion effect is well known in polymer/diluent systems [1–4]. When the diluent can rapidly diffuse away from a growing spherulite because of its large mobility, a concentration gradient is established at the growth front. The existence of a concentration gradient has been confirmed by the concentration distribution observed by ultraviolet microscopy [5,6] and indirectly by the growth rate depending on the distribution of the spherulites [4]. Because of the existence of the concentration gradient, the crystallization kinetics is nonlinear; i.e., the spherulite growth rate is constant at the beginning but decreases at the later stages. In polymer/carbon dioxide (CO_2) systems, characteristic porous structures with various shapes and sizes were obtained due to the exclusion of CO_2 from the crystal growth front to the intercrystalline amorphous region and the growth of bubbles by the supersaturation of CO_2 in the constrained amorphous region [7,8].

On the other hand, in polymer/polymer systems, the mobility of the noncrystalline polymer is small. Thus, the noncrystalline polymer seems to be excluded only on the scale of lamellar bundles, at most. The spherulite becomes coarse and open when the noncrystalline polymer diffuses out of the interlamellar region and is trapped in pockets between lamellar bundles [1,2,5,6,9–13]. Here coarse spherulite has lamellar bundles with relatively large cross section and open spherulite has lamellar bundles separated to a relatively greater extent by noncrystalline components. The increase in openness frequently accompanies with the increase in coarseness [1]. Increasing the fraction of noncrystalline polymer or raising the crystallization temperature (T_C) causes the spherulite morphology to become coarser and more open, while reducing the fraction of noncrystalline polymer or lowering the crystallization temperature causes it to become more compact. Exclusion of noncrystalline polymer from the interlamellar amorphous region in the coarse spherulite was confirmed by small-angle X-ray scattering experiments [12]. In the compact spherulites, various lamellar structures were obtained because of the exclusion of the noncrystalline polymer to the interlamellar amorphous region; e.g., a short, zigzag-type lamellar structure was obtained in high density polyethylene/polyethylene-poly(ethylene-co-butene)-polyethylene block copolymer blends [14]. The development of the crosshatch structure of polypropylene was suppressed in PP/hydrogenated polybutadiene blends [15].

* Corresponding author. Tel./fax: +81 42 388 7294.
E-mail address: hsaitou@cc.tuat.ac.jp (H. Saito).

0032-3861/$ – see front matter © 2010 Elsevier Ltd. All rights reserved.
doi:10.1016/j.polymer.2010.01.055

The amount of the excluded noncrystalline polymer should be changed with time during the spherulite growth due to the change in the concentration at the crystal growth front. The change of the exclusion will cause the morphology change with the distance from the center of the spherulite. However, so far, the discussion about the exclusion effect has been limited on the overall crystalline morphology, and the exclusion effect on the morphology development and the morphology changes in the spherulite have not been elucidated. In this paper, in order to elucidate the exclusion effect on the morphology development, we performed time-resolved light scattering measurements during the crystallization of coarse spherulites and compact ones in poly(vinylidene fluoride) (PVDF)/poly(methyl methacrylate) (PMMA) blends using a highly sensitive charge-coupled device (CCD) camera system. The morphology change with the distance from the center of the spherulite caused by the characteristic morphology development is discussed by the results of atomic force microscopy (AFM).

2. Experimental

The polymer specimens used in this study were commercial products. PVDF (KF1000, $M_w = 2.5 \times 10^5$ g/mol, $M_n = 1.1 \times 10^5$ g/mol, $M_w/M_n = 2.27$) and PMMA (Acrypet M001, $M_w = 11.0 \times 10^4$ g/mol, $M_n = 5.0 \times 10^4$ g/mol, $M_w/M_n = 2.2$) were supplied by Kureha Chemical Industry Co., Ltd. and Mitsubishi Rayon Co., Ltd., respectively, and were used without further purification.

PVDF and PMMA were dissolved in *N*,*N*–dimethyl acetamide with a total weight concentration of 8 wt%. The blend ratio by weight was fixed at 70/30 (PVDF/PMMA). The solutions were cast onto a cover glass, and the solvents were evaporated under a reduced pressure of 10^{-2} mmHg at room temperature. The cast films were further dried under vacuum (10^{-4} mmHg) at room temperature for 3 days and then at 120 °C for 24 h to completely remove any residual solvent.

The film specimen thus prepared (ca. 30 μm thick) was melted at 220 °C for 10 min in a hot stage. The melt specimen was then rapidly transferred into another hot stage for light scattering measurements, which was set at the aimed crystallization temperature. A polarized He–Ne laser with a wavelength of 632.8 nm was applied vertically to the film specimen. We employed Hv geometry in which the optical axis of the analyzer was set perpendicularly to that of the polarizer [16]. The scattered light passed through the analyzer and then onto a highly sensitive charge-coupled device (CCD) camera with 576 × 382 pixels (Princeton Instruments, Inc., TE/CDD-512-TKM-1), which enables time-resolved measurement with one-dimensional scattering data in a time scale of 0.14 s [17]. The input data from the CCD camera was digitized by an ST-13X controller and was stored in a personal computer for further analysis.

After being kept at T_C for 5 h to ensure complete crystallization and volume-filled spherulites, the specimen was quenched in a water bath at 20 °C. An Olympus BH-2 polarized microscope equipped with an Olympus PM-20 exposure control unit was used to observe the spherulitic morphology. The specimen was then rinsed by acetone under vigorous shaking for 24 h to remove the PMMA-rich amorphous region. The height image of the etched specimen was obtained by atomic force microscopy (AFM; Seiko Instruments SPI3600). The spatial resolutions in the horizontal and vertical directions were 0.1 and 0.05 nm, respectively. Si_3N_4 was used as a cantilever to scan the surface. Tip motion was monitored by light deflected from the cantilever.

SAXS measurements were performed by using NANO-Viewer system (Rigaku Co., Japan). A Cu-Ka radiation (46 kV, 60 mA) was generated and collimated by a confocal max-flux mirror system. The wavelength and the sample to the detector distance were 0.154 nm and 700 mm, respectively. An imaging plate (IP) (Fujifilm BAS-SR 127) was used as a two-dimensional detector and the IP reading device (R-AXIS Ds3, Rigaku Co.) was used to transform the obtained image into the text data.

3. Results and discussion

Fig. 1 shows typical spherulite morphologies of neat PVDF and 70/30 PVDF/PMMA observed by a polarized optical microscope. In neat PVDF, compact spherulites with a clear Maltese-cross pattern were obtained (Fig. 1a). On the other hand, in the blends crystallized at higher T_C above 152 °C in this composition, coarse spherulites developed (Fig. 1b). The coarse spherulites consisting of lamellar bundles with a large cross section and a Maltese-cross pattern is completely lost, suggesting random arrangement of

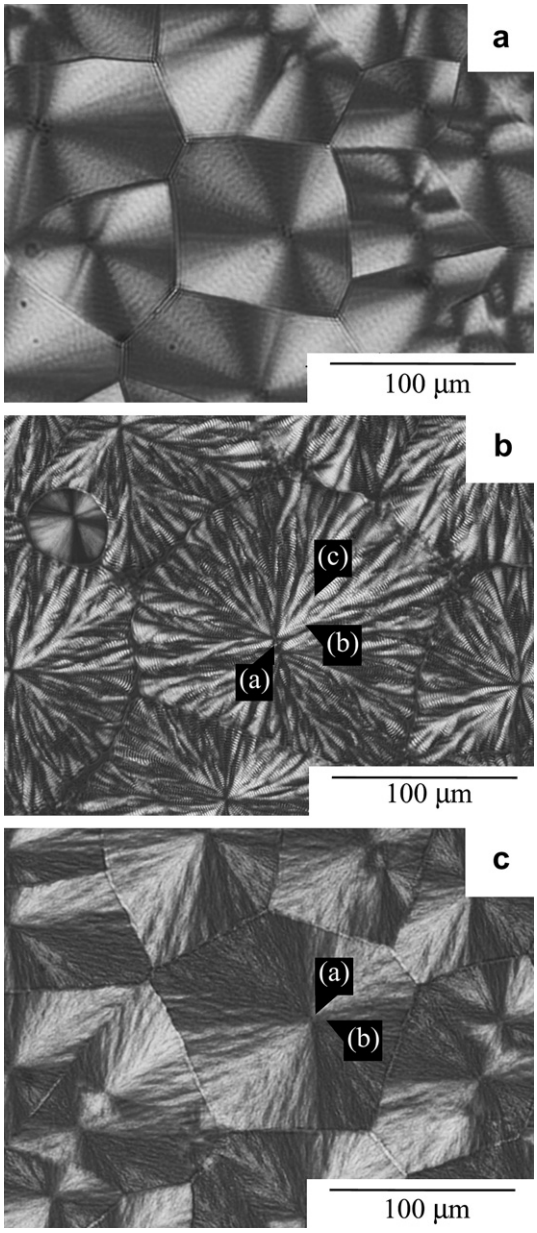

Fig. 1. Polarized optical micrographs: (a) neat PVDF crystallized at T_C of 155 °C, (b) coarse spherulite; 70/30 PVDF/PMMA crystallized at high T_C of 162 °C, (c) compact spherulite; 70/30 PVDF/PMMA crystallized at low T_C of 148 °C. AFM images shown in Figs. 5 and 8 were observed at the labeled regions in Fig. 1(b) and (c), respectively.

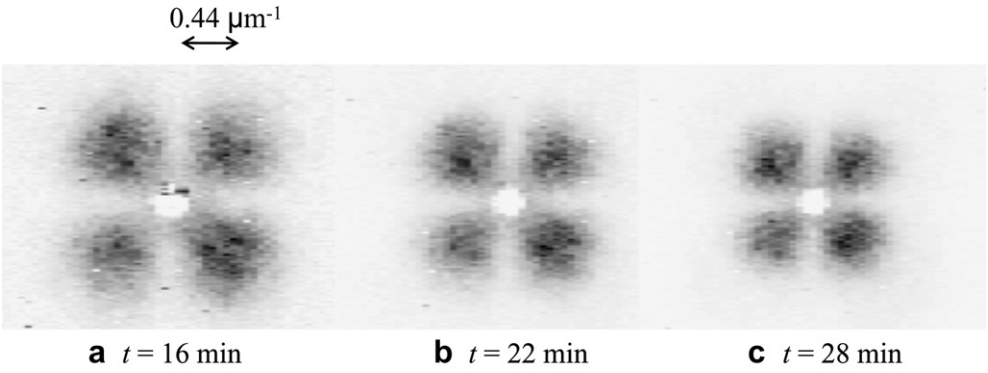

Fig. 2. A series of Hv light scattering patterns of 70/30 PVDF/PMMA during the crystallization at T_C of 162 °C.

lamellar bundles. An extinction concentric ring pattern is also seen. Morra and Stein suggested that the random arrangement of the lamellar bundles is caused by the exclusion of PMMA from the lamellar bundles during crystal growth; i.e., the excluded PMMA hinders the radial growth of the crystalline lamellae [18,19]. Extinction region exists between lamellar bundles, suggesting that the spherulite is open and lamellar bundles are separated by the excluded PMMA. The exclusion of PMMA from the lamellar bundles was confirmed by the small-angle X-ray scattering experiments [12]. In the blends crystallized at lower T_C below 152 °C in this composition, compact spherulites similar to those of neat PVDF were obtained (Fig. 1c). Although overview of the compact spherulites is similar to that of the neat PVDF, the Maltese-cross patterns are diffuse, indicating that mottled regions exist where polarized light is transmitted at 0° and 90°. Thus, it is considered that lamellar bundles in the compact spherulites are arranged more randomly than that in neat PVDF.

Fig. 2 shows the change of the Hv light scattering patterns during the crystallization of 70/30 PVDF/PMMA at 162 °C. The Hv scattering patterns were the four-leaf clover type, which are characteristic of spherulites. The four-leaf clover pattern became smaller with time. As expected from the four-leaf clover pattern, the one-dimensional scattering profile at an azimuthal angle of 45° in the two-dimensional scattering pattern had a maximum at a scattering angle of θ_m. From θ_m, the average radius of the spherulites (R_{Hv}) can be estimated by [16]

$$4.09 = 4\pi(R_{Hv}/\lambda)\sin(\theta_m/2) \quad (1)$$

where λ is the wavelength of light in the specimen. Hence, the four-leaf clover pattern becomes smaller and θ_m decreases as the radius of the spherulite becomes larger during crystallization.

Fig. 3 shows the estimated radii R_{Hv} of (a) neat PVDF and (b) 70/30 PVDF/PMMA as a function of crystallization time obtained at various T_C's by the light scattering results using Eq. (1). Here, the R_{Hv} values are limited below 35 μm because of the low accuracy for the larger R_{Hv}, which is obtained in the very small-angle region below 0.5°. A linear growth in the size of the spherulite with time is seen in neat PVDF, as reported for other neat polymers (Fig. 3a). The interesting result here is that nonlinear and discontinuous growth behavior is seen in PVDF/PMMA blends at high crystallization temperatures above 152 °C in which the coarse spherulites shown in Fig. 1b are obtained, while linear growth behavior is seen at a low T_C of 148 °C in which the compact spherulites shown in Fig. 1c are obtained (Fig. 3b). At 162 °C, R_{Hv} increases linearly with time at the early stages, but the rate of growth decreases discontinuously at time t_1, which is marked with an arrow in Fig. 3b. After a short interval, R_{Hv} starts to increase at time t_2, and nonlinear growth behavior is seen after t_2; i.e., the rate of growth decreases with time after t_2. That is, a two-step process of crystallization occurs during the development of the coarse spherulite.

Here, two possible origins for the nonlinear growth behavior are considered. One is collision of the neighboring spherulites; the other is hindrance of crystal growth by the excluded PMMA at the crystalline growth front. As shown in Fig. 1b, the coarse spherulites collide when their radii are about 100 μm. However, Fig. 3b shows that the radii of the spherulites are only 25 μm at the time of the onset of nonlinear growth, t_2. These results suggest that the nonlinear growth behavior at high T_C is not caused by the collision of neighboring spherulites. Therefore, the origin of the nonlinear growth behavior could be attributed to the hindrance of the crystal growth by the excluded PMMA on the melt–crystal interface, which will be discussed in detail in the following text.

According to a model calculation of the scattering profiles proposed by Yoon and Stein [20], the broadening of the one-

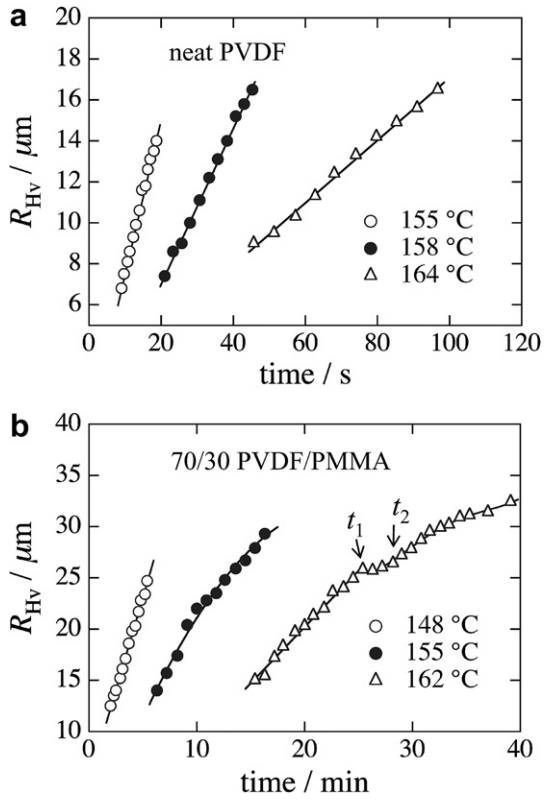

Fig. 3. Time variation of the spherulite radius, R_{Hv}, crystallized at various T_C's: (a) neat PVDF, (b) 70/30 PVDF/PMMA.

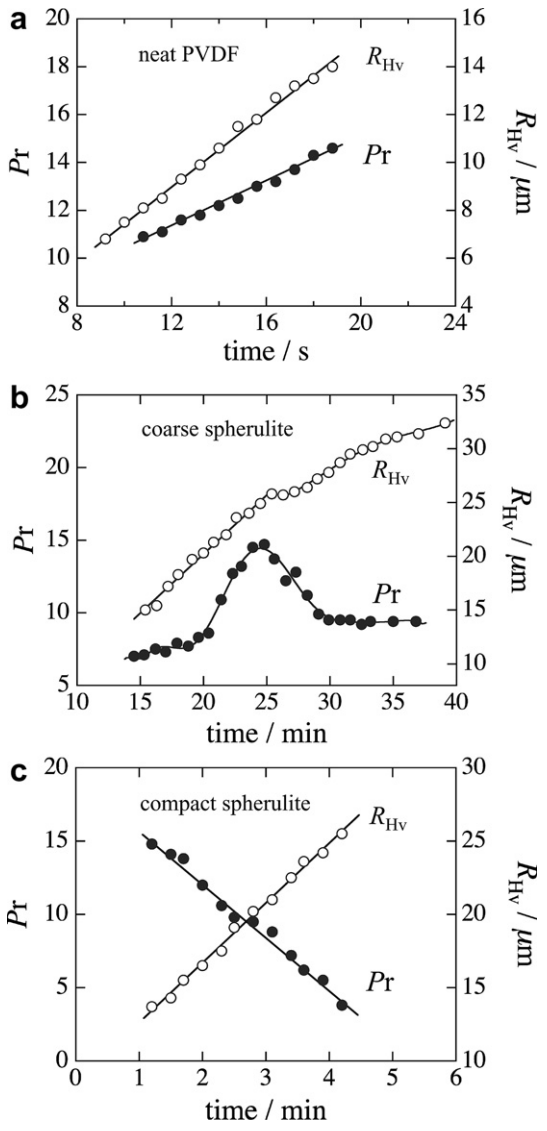

Fig. 4. Time variation of the order parameter, *Pr*, and the spherulite radius, R_{Hv}: (a) neat PVDF crystallized at T_C of 155 °C, (b) 70/30 PVDF/PMMA crystallized at T_C of 162 °C, (c) 70/30 PVDF/PMMA crystallized at T_C of 148 °C.

dimensional Hv light scattering profile is attributed to the orientation fluctuation of the optic axis within a spherulite. Hence, by the Hv light scattering profile, one can also discuss the ordering within the spherulite on a submicrometer scale. In order to discuss the ordering process inside the spherulite, it is convenient to employ an order parameter (*Pr*). The relative intensity of scattered light at wide-angle regions ($\theta < \theta_m$) decreases by the decrease of the orientation fluctuation in the radial direction; i.e., *Pr* increases with increasing the degree of the ordering in the spherulite. *Pr* could be given by using the reduced scattering angle (w) [20–22]:

$$w = (2\pi/\lambda)\cdot R_{Hv}\cdot \sin\theta. \quad (2)$$

then, *Pr* is defined by the ratio of the intensity (I) at $w = 4$ to that at $w = 8$:

$$Pr = I(w = 4)/I(w = 8) \quad (3)$$

Fig. 4 shows the calculated order parameter *Pr* as a function of crystallization time in (a) neat PVDF at T_C of 155 °C, (b) coarse spherulite of the blends at T_C of 162 °C, and (c) compact spherulite of the blends at T_C of 148 °C. Spherulite radii R_{Hv} are also shown in Fig. 4 for comparison. In the neat PVDF, *Pr* increases monotonically with crystallization time associated with the increasing R_{Hv} (Fig. 4a). This result suggests that the disordered crystalline domain with low crystallinity is formed at the early stages, and it grows to yield the spherulite by increasing its size and the degree of ordering, as demonstrated in the crystallization of polypropylene and poly(ethylene terephthalate) [17,23,24].

On the other hand, such a monotonic time dependence of *Pr* is not seen in the coarse spherulites of the blends (Fig. 4b). *Pr* increases with time at the early stages and then decreases at the later stages. That is, a two-step process of crystallization is also seen in terms of *Pr*. The nonlinear growth associated with the decreased *Pr* is characteristic of the coarse spherulite. The decrease in *Pr* during the crystal growth is attributed to the irregularly arranged lamellar bundles; i.e., the arrangement of the lamellar bundles becomes more irregular during the growth of the spherulite. Since the irregularly arranged lamellar bundles are formed due to the hindrance of crystallization by the excluded PMMA, the decrease in *Pr* might be attributed to the increase in the amount of the excluded PMMA at around the growth front as the spherulite grows. Of particular interest is that the ordering starts to decrease at around t_2 when the nonlinear growth of the spherulites starts. Because of the existence of the concentration gradient at the growth front induced by the large amount of excluded PMMA, the rate of spherulite growth decreases and the crystallization kinetics become nonlinear due to the diffusion-controlled process [1–4].

In the compact spherulites of the blends, *Pr* decreases monotonously with time during the spherulite growth (Fig. 4c). The change in *Pr* is opposite to that obtained in the neat PVDF, while the overview of the spherulites is almost similar to that of the neat PVDF as shown in Fig. 1. The result suggests that the arrangement of the lamellar bundles becomes more irregular during the growth of the spherulite. The increase in the irregularity might be attributed to the increase in the amount of excluded PMMA at around the growth front during spherulite growth, as demonstrated in the coarse spherulite. Although *Pr* decreases with time, R_{Hv} linearly increases. This might imply that no large concentration gradient is formed at around the growth front in the compact spherulite.

The exclusion of PMMA can be quantitatively discussed in terms of parameter δ, as suggested by Keith and Padden [1,2]:

$$\delta = D/G \quad (4)$$

where δ is the distance in which the noncrystalline component can be excluded from the crystal growth front, D is the diffusion coefficient of the noncrystalline component (PMMA), and G is the rate of growth of the crystalline polymer (PVDF). As the temperature becomes lower, D decreases and G increases, so that δ decreases. This suggests that the amount of excluded PMMA in the compact spherulite obtained at a lower temperature is smaller than that in a coarse spherulite obtained at a higher temperature. Because of the smaller amount of excluded PMMA in the compact spherulite, no large concentration gradient is formed at around the growth front and no nonlinear spherulite growth behavior is observed.

Fig. 5 shows the AFM height images of the coarse spherulite obtained at T_C of 162 °C for the three regions labeled in Fig. 1b. For explanation, the hierarchical structure inside the coarse spherulite is schematically shown in Fig. 6. Since AFM observation was performed after extraction of PMMA by etching with acetone, the remaining material should only be PVDF. Thus white stripes having a length of ca. 1.5 μm and width of ca. 0.1 μm seen in the AFM images are assigned to PVDF. As shown in Fig. 7, a peak was observed in the Lorentz-corrected SAXS profiles of the blends, suggesting regular arrangement of crystalline lamellae. The

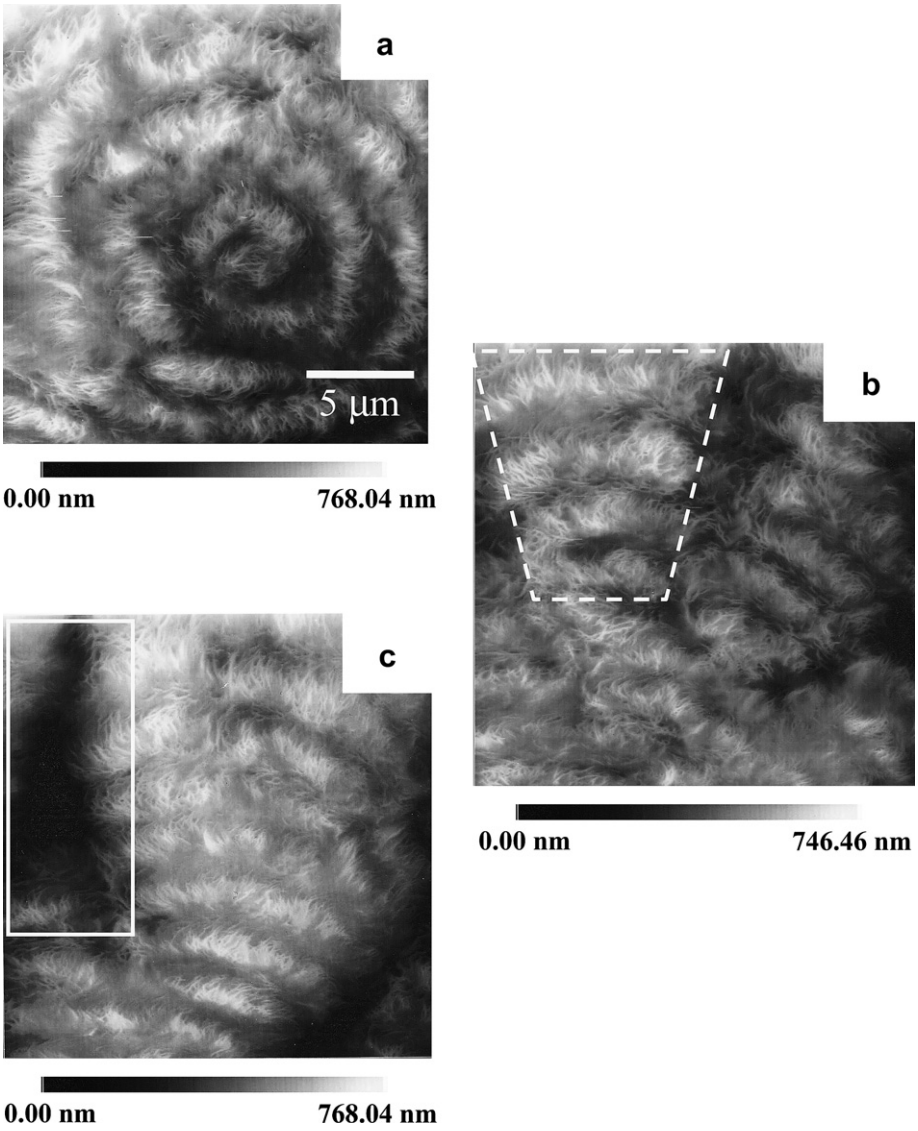

Fig. 5. AFM height images of the coarse spherulites in 70/30 PVDF/PMMA crystallized at T_C of 162 °C. Images (a) – (c) are viewed at regions labeled (a) – (c) in Fig. 1b. The trapezoidal area drawn by the broken white stripes in (b) indicates bundles of lamellar stacks. The rectangular area drawn by the solid white lines in (c) indicates amorphous pocket of excluded PMMA. The scale bar shown below the image represents the height of the concave surface of the spherulite.

periodic distance of the elemental lamellae, L, calculated by using the Bragg's law ($L = 2\pi/q_{max}$), in which q_{max} is the scattering vector of peak maximum, was 0.026 μm for the coarse spherulite. Since the periodic distance of the elemental lamellae is much smaller than the width of the white stripes seen in the AFM images, the white stripes are not assigned to lamellae but to lamellar stacks consisting of several elemental lamellae; i.e., the lamellar stacks consist of about 3–4 elemental 1amellae.

As shown in Fig. 5a, as is often observed in other spherulite species [1,25,26], a spiral structure is seen at the core of the coarse spherulite. The concentration of the lamellar stacks in the ridge is greater than that in the valleys, and the lamellar stacks are discontinuous in the radial direction. The concentration difference might be attributed to the exclusion of PMMA during crystallization; i.e., PMMA is excluded from the PVDF-rich crystallized ridge into the PVDF-poor interspiral valley. The periodic arrangement of the lamellar stacks in the radial and tangential directions corresponds to the extinction concentric ring pattern shown in Fig. 1b. The spiral and discontinuous structure is caused by rhythmic crystal growth [1,26] theoretically explained by the time-dependent Ginzburg–Landau equation considering the coupling of compositional ordering and orientational crystal ordering [27].

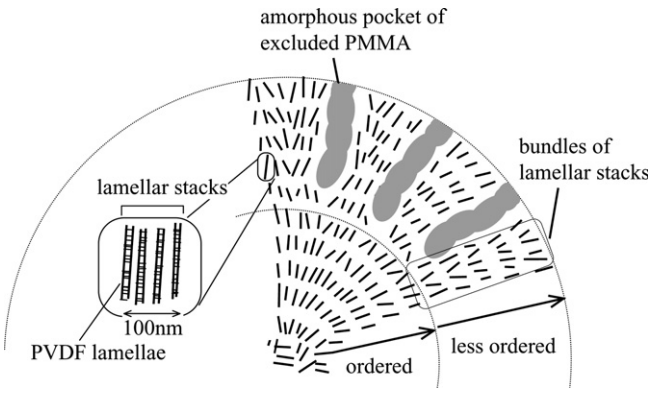

Fig. 6. Schematic diagram of the coarse spherulite shown in Fig. 5.

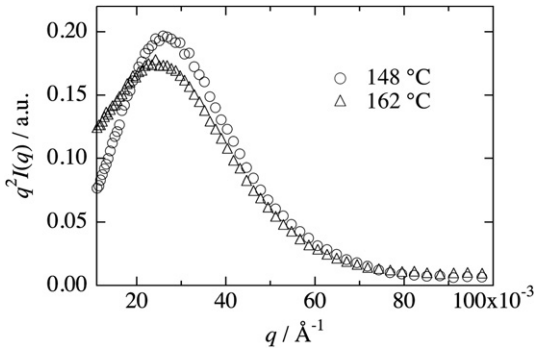

Fig. 7. Lorentz-corrected SAXS profiles of 70/30 PVDF/PMMA crystallized at various T_C's.

Arrangement of the lamellar stacks is disordered at around the center of the coarse spherulite. The ordering of the lamellar stacks in the radial direction becomes greater as the distance from the center increases (Fig. 5a). This AFM image supports the results obtained by time-resolved light scattering measurements that *P*r increases with time at the early stages. At the outer region above ca. 20 μm from the center, the lamellar stacks are regularly arranged and the higher-order bundles are seen, as indicated by the trapezoid drawn with a broken white line in Fig. 5b and schematically shown in Fig. 6. The bundles of lamellar stacks formed at the outer region are irregularly arranged as the distance from the center increases, while the arrangement of the lamellar stacks inside the bundles is almost same. The irregularly arranged lamellar bundles with large cross sections shown in Fig. 1b are assigned to the irregularly arranged bundles of lamellar stacks. Since the irregularity of the lamellar bundles is seen at the outer region above ca. 20 μm from the center and the decrease in *P*r is seen when the spherulite grows to the radius of ca. 25 μm, it is considered that the decrease in *P*r at the late stages demonstrated in Fig. 4b is attributed to the irregular arrangement of the bundles of lamellar stacks.

Wide and deep holes with a width of ca. 3 μm and depth of ca. 0.5 μm are seen between the bundles of lamellar stacks in the coarse spherulite, as indicated by the square drawn with a solid white line in Fig. 5c. This hole is attributed to an amorphous pocket of PMMA extracted by the etching with the solvent, as schematically shown in Fig. 6. Owing to the existence of the large amorphous pocket, the spherulite is open as shown in Fig. 1b. This result suggests that PMMA is excluded into the pocket area during crystallization. The amorphous pockets become larger as the distance from the center increases, suggesting that the amount of excluded PMMA increases as the distance from the center increases. Because of the physical hindrance of the crystallization by the large amorphous pocket on a micrometer scale, the bundles of lamellar stacks are irregularly arranged, causing a decrease in *P*r at the later stages, as shown in Fig. 4b. Simultaneously, the large amount of excluded PMMA from the large bundles of lamellar stacks induces a concentration gradient at the melt–crystal interface, which subsequently causes a decrease in the rate of spherulite growth. These results also suggest that formation of the coarse spherulites would originate from the existence of such large amorphous pockets and the subsequent irregular arrangement of the bundles of lamellar stacks.

Fig. 8 shows AFM height images of the compact spherulite obtained at a T_C of 148 °C for the two regions labeled in Fig. 1c. The hierarchical structure inside the compact spherulite is schematically shown in Fig. 9. The size of the lamellar stacks in the compact spherulites is almost the same as that of the coarse spherulites. The length and width of the lamellar stacks are ca. 1.5 μm and ca. 0.1 μm, respectively. Since the periodic distance of the elemental lamellae calculated by SAXS profile in Fig. 7 is 0.024 μm, the lamellar stacks in the compact spherulite consist of about 3–4 elemental lamellae. As shown in Fig. 7, the differences of the shape and peak position of the SAXS profiles obtained at different *T*c's are small, suggesting that the differences of the arrangement and periodic distance of lamellae in the compact spherulite and coarse one are small, thought the arrangement and size of the lamellar bundles are quite different. The bundles of lamellar stacks in the compact spherulite are arranged in a radial direction like maple leaves, as indicated by the trapezoids drawn with broken white lines in Fig. 8b. The bundles of lamellar stacks in the compact spherulites are much smaller than those in the coarse spherulite. This might explain the

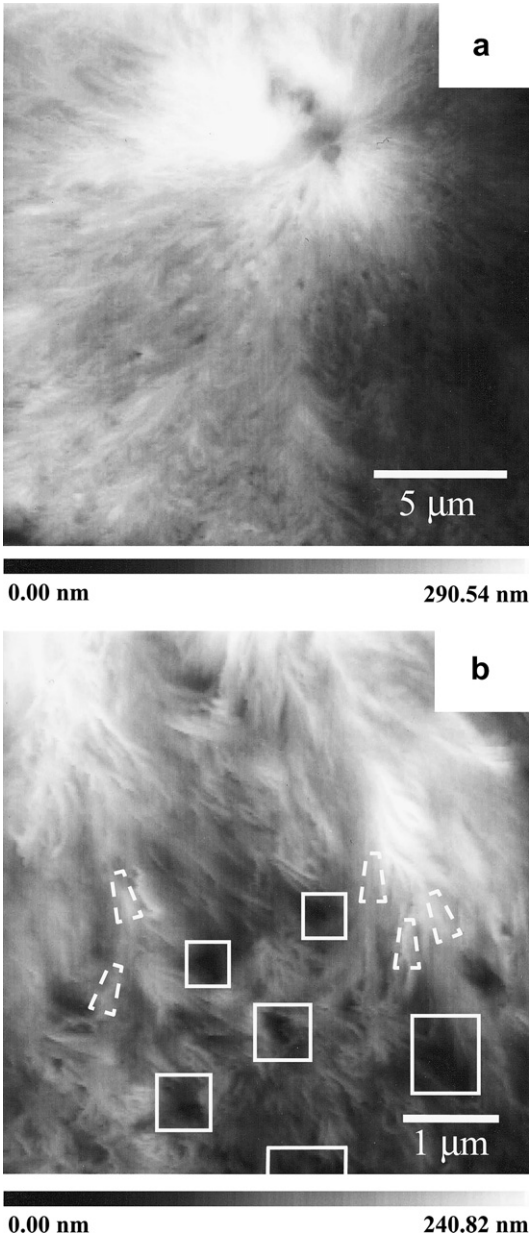

Fig. 8. AFM height images of the compact spherulites in 70/30 PVDF/PMMA crystallized at T_C of 148 °C. Images (a) and (b) are viewed at regions labeled (a) and (b) in Fig. 1c. The trapezoidal area drawn by the broken white stripes in (a) indicates bundles of lamellar stacks. The rectangular areas drawn by the solid white lines in (b) indicate amorphous pockets of excluded PMMA. The scale bar shown below the image represents the height of the concave surface of the spherulite.

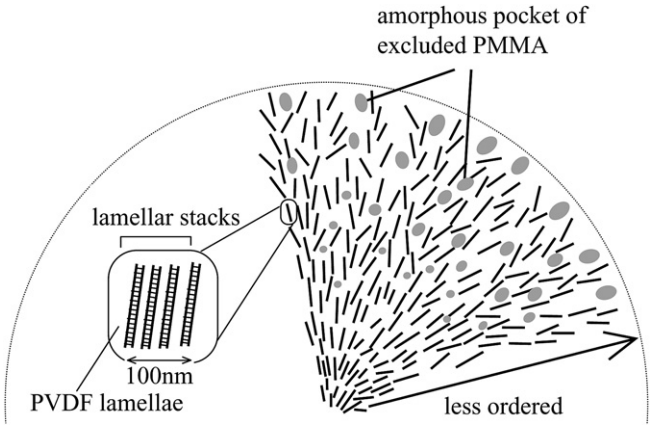

Fig. 9. Schematic diagram of the compact spherulite shown in Fig. 8.

different size of the cross section of the lamellar bundles shown in Fig. 1; i.e., the cross section of the compact spherulites shown in Fig. 1c is much smaller than that of the coarse spherulites shown in Fig. 1b.

At around the center of the compact spherulite, the color depth is high, suggesting that the concentration of PVDF is high and that the lamellar stacks are tightly packed (Fig. 8a). The color depth decreases as the distance from the center increases, suggesting that the concentration of the lamellar stacks decreases because the distance from the center increases. At the outside of the core, small holes with a width of ca. 1 μm and a depth of ca. 0.5 μm are seen between the bundles of lamellar stacks, as indicated by the squares drawn with solid white lines in Fig. 8b. The holes become larger as the distance from the center increases. Since these holes originated from the amorphous pockets of the PMMA extracted by the solvent etching, as mentioned above, it is considered that the amorphous pockets are formed by the excluded PMMA in the region between the bundles of lamellar stacks, as schematically shown in Fig. 9. The amorphous pockets of PMMA in the compact spherulites obtained at lower temperatures are much smaller than those in the coarse spherulites obtained at higher temperatures, as expected from Eq. (4). The mottled regions shown in Fig. 1c indicate the amorphous pockets of the excluded PMMA. The amorphous pockets of the excluded PMMA become larger and the arrangement of the bundles of lamellar stacks becomes irregular. This suggests that the compact spherulite grows as the regularity of the lamellar bundles associated with the increased number of excluded PMMA domains decreases. This might explain the large monotonic decrease in *P*r demonstrated in Fig. 4c. The decrease of *P*r in the compact spherulite is much larger than that in the coarse spherulite; i.e., *P*r decreases from 15 to 4 in the compact spherulite while it decreases from 15 to 10 in the coarse spherulite. Since the *P*r decreases as the orientation fluctuation in the radial direction increases, this suggests that the growth direction of the small lamellar bundles in the compact spherulite fluctuates to a greater extent than that of the large lamellar bundles in the coarse spherulite.

4. Conclusion

AFM observation of the crystallized PVDF/PMMA blends revealed that amorphous pockets of PMMA exist between bundles of lamellar stacks due to the exclusion of PMMA from the crystal growth front, and they are larger as the distance from the spherulite center increases. The sizes of the amorphous pockets are on a micrometer scale in the coarse spherulite obtained at high temperatures, while they are small on a submicrometer scale in the compact spherulite obtained at low temperatures. The results suggest that the amount of excluded PMMA increases as the distance from the spherulite center increases and the crystallization temperature becomes higher. The exclusion of PMMA and the formation of the amorphous pockets at the crystal growth front induce characteristic crystallization behavior; the growth rate decreases and the ordering in the spherulite decreases during spherulite growth.

Acknowledgment

This work was partially supported by the Japan Society for the Promotion of Science (Grant-in-Aid for Scientific Research, No. 20350101).

References

[1] Keith HD, Padden FJ. J Appl Phys 1963;34:2409.
[2] Keith HD, Padden FJ. J Appl Phys 1964;35:1270.
[3] Goldenfeld N. J Cryst Growth 1987;84:601.
[4] Okada T, Saito H, Inoue T. Macromolecules 1990;23:3865.
[5] Ryan TG, Calvert PD. Polymer 1982;23:877.
[6] Calvert PD, Billingham NC. Appl Polym Light Microscopy: Elsevier Appl Sci; 1989 [chapter 7].
[7] Koga Y, Saito H. Polymer 2006;47:7564.
[8] Fukasawa Y, Chen J, Saito H. J Polym Sci Part B: Polym Phys 2008;46:843.
[9] Warmer FP, MacKnight WJ, Stein RS. J Polym Sci Polym Phys 1977;15:2113.
[10] Stein RS, Khambatta FB, Warmer FP, Russell T, Escala A, Balizer E. J Polym Sci Polym Symp 1978;63:313.
[11] Hudson SD, Davis DD, Lovinger A. Macromolecules 1992;25:1759.
[12] Saito H, Stühn B. Macromolecules 1994;27:216.
[13] Braun D, Jacobs M, Hellmann GP. Polymer 1994;35:706.
[14] Takagi S, Saito H, Chiba T, Inoue T, Takemura Y. Polymer 1998;39:1643.
[15] Svoboda P, Saito H, Chiba T, Inoue T, Takemura Y. Polym J 2000;32:915.
[16] Stein RS, Rhodes MB. J Appl Phys 1960;31:1873.
[17] Lee CH, Saito H, Inoue T. Macromolecules 1993;26:6566.
[18] Morra BS, Stein RS. J Polym Sci Polym Phys 1982;20:2243.
[19] Morra BS, Stein RS. J Polym Sci Polym Phys 1982;20:2261.
[20] Yoon DY, Stein RS. J Polym Sci Polym Phys 1974;12:763.
[21] Stein RS, Chu W. A-2. J Polym Sci 1970;8:1137.
[22] Stein RS, Misra A, Yuasa T, Khambatta F. Pure Appl Chem 1977;49:915.
[23] Okada T, Saito H, Inoue T. Macromolecules 1992;25:1908.
[24] Lee CH, Saito H, Inoue T. Macromolecules 1996;29:7034.
[25] Ryschenkow G, Faivre G. J Cryst Growth 1988;87:221.
[26] Okabe Y, Kyu T, Saito H, Inoue T. Macromolecules 1998;31:5823.
[27] Kyu T, Chiu H-W, Guenthner AL, Okabe Y, Saito H, Inoue T. Phys Rev Lett 1999;83:2749.